Thrust Vectoring Control of Supersonic Flow Through an Orifice Injector

Ibrahim Mnafeg, Azgal Abichou, Lotfi Beji

Abstract—Traditional mechanical control systems in thrust vectoring are efficient in rocket thrust guidance but their costs and their weights are excessive. The fluidic injection in the nozzle divergent constitutes an alternative procedure to achieve the goal. In this paper, we present a 3D analytical model for fluidic injection in a supersonic nozzle integrating an orifice. The fluidic vectoring uses a sonic secondary injection in the divergent. As a result, the flow and interaction between the main and secondary jet has built in order to express the pressure fields from which the forces and thrust vectoring are deduced. Under various separation criteria, the present analytical model results are compared with the existing numerical and experimental data from the literature.

Keywords—Flow separation, Fluidic thrust vectoring, Nozzle, Secondary jet, Shock wave.

NOMENCLATURE

NPR   Nozzle pressure ratio ($\frac{P_{0i}}{P_a}$).
SPR   Secondary pressure ratio ($\frac{P_{0j}}{P_{0i}}$).
P_{0i} Chamber stagnation pressure.
P_{0j} Second injection pressure.
P_a Ambient pressure.
P_p Plateau pressure.
P Isentropic pressure.
P_b The pressure at the hyperbolic surface.
C_d Discharge Coefficient.
δ Deviation angle.
$F_{x,y}$ Force components in x and y direction.
F_j Second injection reactive force.
$\vec{F_c}$ Primary flow reactive force (Dynalpy flux).
x Nozzle axis with coordinate beginning at the nozzle throat.
x_t Divergent length of the nozzle.
x_m x-coordinate of the secondary injection port.
x_d x-coordinate of the end of the secondary injection port.
x_e x-coordinate of the end of the nozzle.
A_c Surface of the throat of the nozzle.
A_{jc} Surface of the orifice.
A_e Surface of the nozzle at the exit.
f_m Mass-flow ratio.
α Divergent conical half-angle.
r Radius of the nozzle at x.
r_c Throat radius.
ψ Angular coordinate.
x_s x-coordinate of the separation point.
Δ Standoff distance.
L_s Curvature radius.
ψ_{Max} Maximum angle to the hyperbolic curve.
ψ_0 Maximum angle to the boundary of the orifice.
γ Heat capacity ration of the primary flow.
γ_j Heat capacity ration of the secondary flow.
M Mach number.

I. INTRODUCTION

THRUST vector control via secondary injection for rocket propulsion systems has been investigated since the 1950s. Using fluidic control in stead of mechanical control system permits to eliminate the kinematic structure and mechanical actuators. Hence, a significant reduction in nozzle weight, cost, and complexities. In the early investigation, jet penetration experiments were performed by Hefner and Sterrett [8], Avduevskii *et al.* [9], and Vlagov *et al.* [10].

There are three main types of fluidic injection: counterflow, coflow, and shock vector control. The investigation here cover Shock Vector Control (SVC) which uses the injection of secondary flow downstream the throat in the diverging section. The circular sonic injection is parametrically analyzed by Shetz and Billig [13] and also by the early researchers on the topic of fluidic thrust vectoring of axisymmetric nozzles such as Nielson *et al.* [14], and Guhse [15]. The secondary fluid injected, creates an unsteady complex three-dimensional flow field inside the nozzle. This complex flow field includes not only a strong bow-shock creating asymmetry and a weak separation shock due to boundary layer separation [16] upstream of the injection location but also a Mach disc and reattachment region accompanied by recompression downstream of the injection orifice as shown in Fig. 1. At the injection port a largely under-expanded secondary flow expands suddenly through the Prandtl-Meyer fan emerging at the edge of injection port and it is naturally surrounded by the barrel shock wave.

The fluidic injection in the divergent of a supersonic nozzle using orifice produces a dissymmetry in the distribution of the pressure at the wall of the nozzle. This distribution depends of the nozzle's regime. A circular transverse sonic injection at the flat plate into supersonic cross-flow is a purely three-dimensional case where flow effects propagation in all three spatial directions.

Compared to three-dimensional numerical calculations, bases on solving the Navier-Stokes equations requiring long calculation time and sometimes prohibitive, the realization of a 3D analytical model becomes necessary in order to reduce the computation burden.

In this paper, we will investigate the fluidic thrust vectoring by SVC using orifice injector in section II. Section III deals

I. Mnafeg is with the LIM Laboratory, Polytechnic School of Tunisia, BP743, 2078 La Marsa, Tunisia. mnafeg_fr@yahoo.fr
A. Abichou is with the LIM Laboratory, Polytechnic School of Tunisia, BP743, 2078 La Marsa, Tunisia. Azgal.Abichou@ept.rnu.tn
L. Beji is with the IBISC-EA4526 Laboratory, University of Evry, 40 rue du Pelvoux, 91020 Evry, France. Lotfi.Beji@ibisc.univ-evry.fr
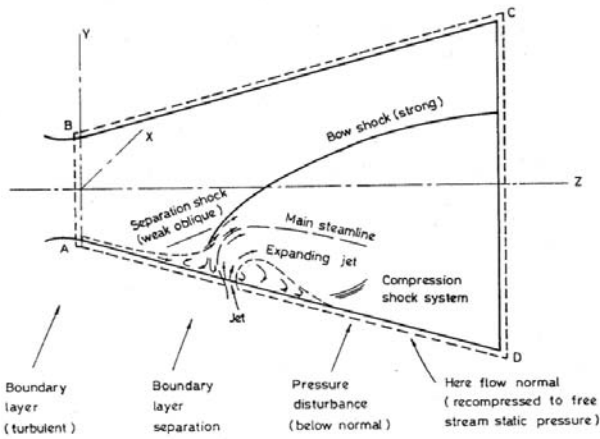
World Academy of Science, Engineering and Technology
International Journal of Aerospace and Mechanical Engineering
Vol:9, No:7, 2015

Fig. 1.   Complex flow structure associated with SITVC [1]
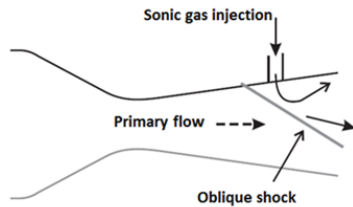
Fig. 2.   Secondary sonic injection thrust vectoring principle.

Fig. 3.   Geometry of the conical nozzle.

Fig. 4.   Zone type's at the wall of the nozzle.

with forces computations including the balance forces for the given flow zones. In section IV, the implementation and validation of our results on a Matlab platform is addressed.

II. ANALYTICAL APPROACH

The analytical model of a fluidic thrust vector is based on the study of the analytical blunt-body model proposed by Spaid and Zukoski [2] [3]. The 2D case has been studied by Mangin [7] and he found that optimal effects are assumingly reached with secondary injection adapted to the plateau pressure of the separation zone. The expression of the penetration height and separation criterion is further improved for ring and circular injection and reported by Maarouf [11] and Sellam [12].

The secondary gas injection into the divergent of a supersonic nozzle leads to shock interaction and separation zone upstream the injection orifice that cause the deviation of the main nozzle flow by an angle δ (Fig. 2). The injected flow acts like a virtual pressure ramp when seen by the primary flow. As the main thrust producing flow passes through this shock it turns away from the injection port (orifice) and by doing such vectors the force produced.

Hence, we can define the deviation angle $\delta = \tan^{-1} \frac{F_y}{F_x}$, where F_x and F_y are forces along x and y directions. We will consider a conical nozzle with throat radius and divergent conical half-angle α (Fig. 3).

With respect to the reference frame $\mathbf{R}(X, Y, Z)$ with the origin assumed to be coincide with the throat center, X is oriented toward the divergent, and the Y is oriented toward
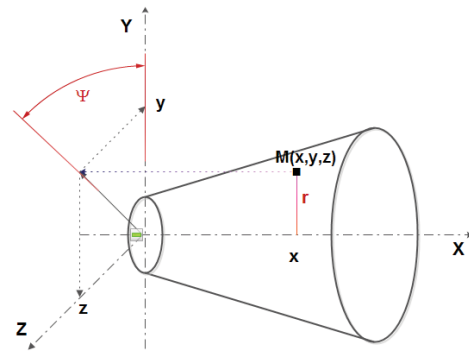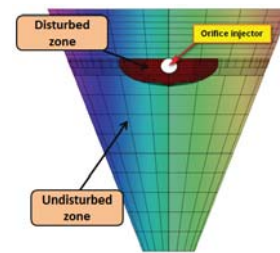
the injector. The surface parametrization of the divergent is:

$$\vec{S} = \begin{pmatrix} x \\ y \\ z \end{pmatrix} = \begin{pmatrix} \frac{r-r_c}{\tan\alpha} \\ r\cos\psi \\ r\sin\psi \end{pmatrix}_{\mathbf{R}}$$

with $r = r_c + x\tan\alpha$.

A surface element $\vec{ds}$ is oriented outward surface $\vec{ds} = ds\vec{n}$ with $\vec{n}$ is the normal vector of the surface S

$$\vec{ds} = \begin{pmatrix} -rdrd\psi \\ r\cos\psi dxd\psi \\ r\sin\psi dxd\psi \end{pmatrix}$$

The phenomena of sonic injection through an orifice produces two types of zone at the wall of the nozzle (Fig.4). The disturbed zone by this sonic injection and it is locate between the abscissa of the separation point x_s and the end of the orifice. The undisturbed zone where the primary flow didn't interact with the secondary jet located at the remain of nozzle's wall.

The analytical model is mainly based on determining the characteristic of the hyperbolic shape of the line delimiting the separation area upstream the injection port. This shape is called separation line which means the separation line of the boundary layer due to the barrier presented by the injected fluid. It will be distributed into several sections: front, around and behind the injection slot. Modeling of this line is also dependent of the operating regime of the nozzle (Fig. 5).

In this paper we will use a conical nozzle with $NPR = 37.5$, so the regime of this nozzle is under-expanded regime. The wall of the nozzle is divided in four parts as shown in Fig. 6:

- Zone 1 (Ω_1): it is undisturbed zone and the pressure is isentropic pressure $P(x)$;
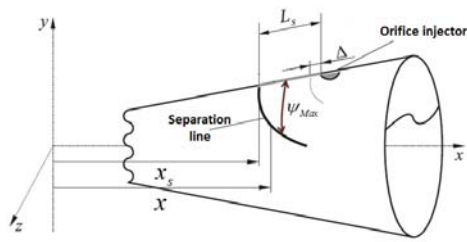
World Academy of Science, Engineering and Technology
International Journal of Aerospace and Mechanical Engineering
Vol:9, No:7, 2015

Fig. 5.   The shape of the separation line.
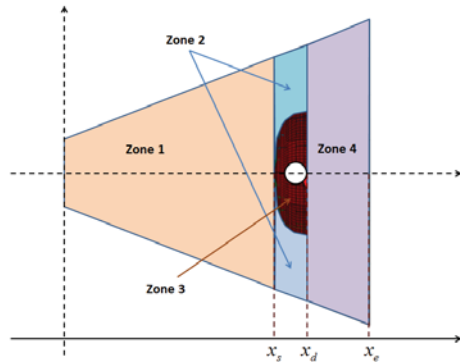
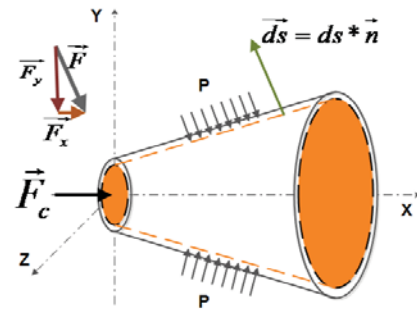Fig. 6.   The different zones at the wall of the nozzle.

Fig. 7.   Forces at the control surface (CS).

component $\vec{F}_y$. For an element surface $\vec{ds}$, the elementary force $d\vec{F}$ is given by $\overrightarrow{dF} = -P(x)ds\vec{n}$, so

$$\overrightarrow{dF} = \left(\begin{array}{c} \overrightarrow{dF}_x \\ \overrightarrow{dF}_y \end{array} \right) = \left(\begin{array}{c} -P(x)ds\vec{n}_x \\ -P(x)ds\vec{n}_y \end{array} \right)$$

- Zone 2 (Ω_2): located at the two sides of the interaction area and the pressure is isentropic pressure $P(x)$;
- Zone 3 (Ω_3): this is the interaction zone and the pressure is $P_b(x, \psi)$;
- Zone 4 (Ω_4): in this area we ignore the reattachment effects of the secondary jet at the wall of the nozzle, so the pressure is isentropic pressure $P(x)$.

where for $i = 1, 4$ the Ω_i set will be defined subsequently. In the undisturbed zone, the pressure is calculated using the isentropic relation, so

$$\frac{P(x)}{P_{0i}} = \left(1 + \frac{1}{2}(\gamma - 1)M^2 \right)^{\frac{\gamma}{1-\gamma}}$$

but in the disturbed zone, the formula of pressure is more complicated. The shape of this zone is hyperbolic curve and we will use the formulas of Billig [4] to calculate the curvature radius of this curve. The pressure is this zone is $P_b(x, \psi)$ and it is a function of the abscissa and the angle ψ .

$$P_b(x, \psi) = (P_p - P(x)) \left(1 - \left(\frac{\psi}{\psi_{Max}} \right)^2 \right)^{\frac{1}{2}}$$

where $P(x)$ is the isentropic pressure and P_p is the plateau pressure calculated using an adequate separation criteria.

III. FORCES COMPUTATION

The geometry of the supersonic nozzle is an important parameter in the calculation of the forces. The force $\vec{F}$ exerted by the pressure P on the control surface S, is divided into two components (Fig. 7): an axial component $\vec{F}_x$ and a normal

The computation of the forces in the zone 1 and zone 4 is done for the whole wall of the nozzle unlike the zone 3 and zone 2. First, we will compute the forces for the zone 1 and zone 4, after, we will calculate these forces for the zone 3 and finally, we will close the computation for the zone 2.

A. Zone 1.

The zone 1 is defined by: $\Omega_1 = \{(x, r, \psi)/0 \leq x \leq x_s, r_c \leq r \leq r_s, 0 \leq \psi \leq 2\pi\}$. First, we will compute the force $\vec{F}_{1x}$ along the x direction:

$$\begin{aligned} \vec{F}_{1x} &= \iint\limits_{zone1} \overrightarrow{dF}_{1x} \\ &= \int_0^{x_s} \int_0^{2\pi} (-P(x))(-rdrd\psi)\vec{i} \\ &= \int_0^{x_s} \int_0^{2\pi} P(x)rdrd\psi\vec{i} \\ &= \int_0^{x_s} P(x)r \left[\int_0^{2\pi} d\psi \right] dr\vec{i} \\ &= 2\pi \int_0^{x_s} P(x)rdr\vec{i} \end{aligned} \qquad (1)$$

World Academy of Science, Engineering and Technology
International Journal of Aerospace and Mechanical Engineering
Vol:9, No:7, 2015

and the force $\vec{F}_{1y}$ along y direction is computed as follow:

$$
\begin{aligned}
\vec{F}_{1y} &= \iint_{zone1} \overrightarrow{dF}_{1y} \\
&= \int_0^{x_s} \int_0^{2\pi} (-P(x))(r\cos\psi dxd\psi)\vec{j} \\
&= -\int_0^{x_s} \int_0^{2\pi} P(x)r\cos\psi dxd\psi \vec{j} \\
&= -\int_0^{x_s} P(x)r \left[\int_0^{2\pi} \cos\psi d\psi\right] dx\vec{j} \\
&= -\int_0^{x_s} P(x)r(\sin 2\pi - \sin 0)dx\vec{j} \\
&= \vec{0} \qquad (2)
\end{aligned}
$$

B. **Zone 4.** This zone is defined by $\Omega_4 = \{(x,r,\psi)/x_d \leq x \leq x_e, r_d \leq r \leq r_e, 0 \leq \psi \leq 2\pi\}$. The force $\vec{F}_{4x}$ along the x direction is given by:

$$
\begin{aligned}
\vec{F}_{4x} &= \iint_{zone4} \overrightarrow{dF}_{4x} \\
&= \int_{x_d}^{x_e} \int_0^{2\pi} (-P(x))(-rdrd\psi)\vec{i} \\
&= \int_{x_d}^{x_e} \int_0^{2\pi} P(x)rdrd\psi \vec{i} \\
&= \int_{x_d}^{x_e} P(x)r \left[\int_0^{2\pi} d\psi\right] dr\vec{i} \\
&= 2\pi \int_{x_d}^{x_e} P(x)rdr\vec{i} \qquad (3)
\end{aligned}
$$

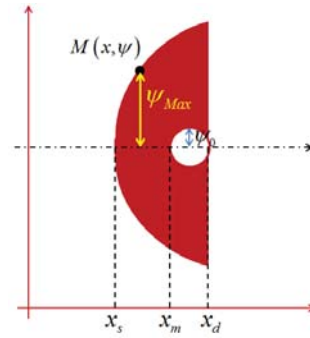and the force along $\vec{F}_{4y}$ direction the y direction is computed

Fig. 8.   The zone 3 parameters.

as follow:

$$
\begin{aligned}
\vec{F}_{4y} &= \iint_{zone4} \overrightarrow{dF}_{4y} \\
&= \int_{x_d}^{x_e} \int_0^{2\pi} (-P(x))(r\cos\psi dxd\psi)\vec{j} \\
&= -\int_{x_d}^{x_e} \int_0^{2\pi} P(x)r\cos\psi dxd\psi \vec{j} \\
&= -\int_{x_d}^{x_e} P(x)r \left[\int_0^{2\pi} \cos\psi d\psi\right] dx\vec{j} \\
&= -\int_{x_d}^{x_e} P(x)r(\sin 2\pi - \sin 0)dx\vec{j} \\
&= \vec{0} \qquad (4)
\end{aligned}
$$

C. **Zone 3.**

This zone is divided into three sub-zones

- zone3-1: $\Omega_{3-1} = \{(x,r,\psi)/x_s \leq x \leq x_m, r_s \leq r \leq r_m, -\psi_{Max} \leq \psi \leq \psi_{Max}\}$.
- zone3-2: $\Omega_{3-2} = \{(x,r,\psi)x_m \leq x \leq x_d, r_m \leq r \leq r_d, \psi_0 \leq \psi \leq \psi_{Max}\}$.
- zone3-3: $\Omega_{3-3} = \{(x,r,\psi)/x_m \leq x \leq x_d, r_m \leq r \leq r_d, -\psi_{Max} \leq \psi \leq -\psi_0\}$.

The Fig 8 explains the different parameters used to identify each sub-zone. The ψ_{Max} and ψ_0 depend only of the x abscissa. So, $\vec{F}_{3x} = \vec{F}31x + \vec{F}32x + \vec{F}33x$

$$
\vec{F}_{3x} = \iint_{zone3-1} \overrightarrow{dF}_{31x} + \iint_{zone3-2} \overrightarrow{dF}_{32x} + \iint_{zone3-3} \overrightarrow{dF}_{33x} \quad (5)
$$

Let us compute these components. The first component,

$$
\begin{aligned}
\vec{F}_{31x} &= \int_{x_s}^{x_m} \int_{-\psi_{Max}}^{\psi_{Max}} (-P_b)(-rdrd\psi)\vec{i} \\
&= \int_{x_s}^{x_m} \int_{-\psi_{Max}}^{\psi_{Max}} P_b rdrd\psi \vec{i}
\end{aligned}
$$

World Academy of Science, Engineering and Technology
International Journal of Aerospace and Mechanical Engineering
Vol:9, No:7, 2015

The second component,

$$\vec{F}_{32x} = \int_{x_m}^{x_d} \int_{\psi_0}^{\psi_{Max}} (-P_b)(-rdrd\psi)\vec{i}$$

$$= \int_{x_m}^{x_d} \int_{\psi_0}^{\psi_{Max}} P_b rdrd\psi\vec{i}$$

The third component,

$$\vec{F}_{33x} = \int_{x_m}^{x_d} \int_{-\psi_{Max}}^{-\psi_0} (-P_b)(-rdrd\psi)\vec{i}$$

$$= \int_{x_m}^{x_d} \int_{-\psi_{Max}}^{-\psi_0} P_b rdrd\psi\vec{i}$$

$$= \int_{x_m}^{x_d} \int_{\psi_0}^{\psi_{Max}} P_b rdrd\psi\vec{i} \qquad (6)$$

Consequently,

$$\vec{F}_{3x} = \int_{x_s}^{x_m} \int_{-\psi_{Max}}^{\psi_{Max}} P_b rdrd\psi\vec{i} + 2\int_{x_m}^{x_d} \int_{\psi_0}^{\psi_{Max}} P_b rdrd\psi\vec{i} \qquad (7)$$

The same procedure will be used to compute $\vec{F}_{3y}$. As a result:

$$\vec{F}_{3y} = \int_{x_s}^{x_m} \int_{-\psi_{Max}}^{\psi_{Max}} P_b r\cos\psi dxd\psi\vec{j} - 2\int_{x_m}^{x_d} \int_{\psi_0}^{\psi_{Max}} P_b r\cos\psi dxd\psi\vec{j} \qquad (8)$$

D. **Zone 2.** This zone is defined by $\Omega_2 = \{(x,r,\psi)/x_s \leq x \leq x_d, r_s \leq r \leq r_d, \psi_{Max} \leq \psi \leq 2\pi - \psi_{Max}\}$
The force $\vec{F}_{2x}$ along the x direction is given by:

$$\vec{F}_{2x} = \iint_{zone2} \vec{dF}_{2x} \qquad (9)$$

Thus,

$$\vec{F}_{2x} = \int_{x_s}^{x_d} P(x)(2\pi - 2\psi_{Max})rdr\vec{i} \qquad (10)$$

and the $\vec{F}_{2y}$ is given by:

$$\vec{F}_{2y} = 2\int_{x_s}^{x_d} P(x)r\sin\psi_{Max})dx\vec{j} \qquad (11)$$

E. **Forces Balance.**
- We have to add to the previous forces two other forces, the first is the dynalpy flux of the primary flow at the throat of the nozzle $\vec{F}_c$ and the second is the reactive force of the secondary flow at the orifice $\vec{F}_j$, then we have:

$$\vec{F}_c = (P_c A_c + \rho_c u_c^2 A_c)\vec{i} = \pi r_c^2 P_c(1+\gamma)\vec{i}$$

where $P_c = P_{0i}(1+\frac{\gamma-1}{2})^{\frac{\gamma}{1-\gamma}}$.
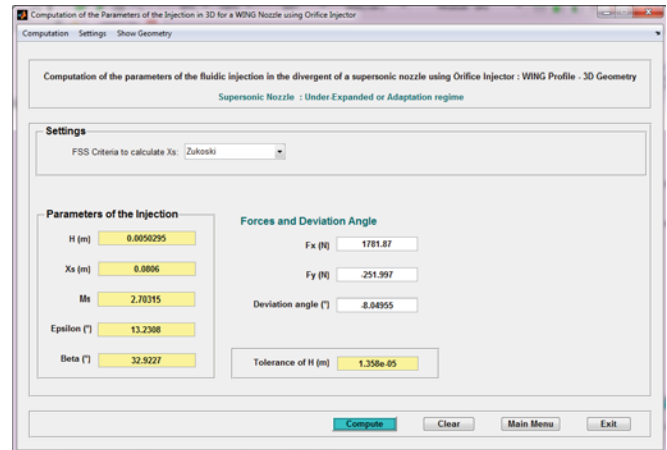The vector of the reactive force of the secondary flow is $\vec{F}_j =$

Fig. 9. Graphical interface of the program.

$F_j(\sin\alpha\vec{i} - \cos\alpha\vec{j})$, with $F_j = C_d A_{jc} P_{jc}(1+\gamma_j)$.
The pressure P_{jc} at the orifice injector is given by: $P_{jc} = P_{0j}(1+\frac{\gamma_j-1}{2})^{\frac{\gamma_j}{1-\gamma_j}}$, and $A_{jc} = \pi\left(\frac{b}{2}\right)^2$
Also, we can define the following components

$$\vec{F}_{jx} = C_d A_{jc} P_{jc}(1+\gamma_j)\sin\alpha\vec{i}$$

and

$$\vec{F}_{jy} = -C_d A_{jc} P_{jc}(1+\gamma_j)\cos\alpha\vec{j}$$

which are necessary to compute the balance forces at the x and y directions.
Now, we may write the following:

$$\vec{F}_x = \vec{F}_{1x} + \vec{F}_{2x} + \vec{F}_{3x} + \vec{F}_{4x} + \vec{F}_c + \vec{F}_{jx}$$

and

$$\vec{F}_y = \vec{F}_{1y} + \vec{F}_{2y} + \vec{F}_{3y} + \vec{F}_{4y} + \vec{F}_{jy}$$

IV. IMPLEMENTATION AND VALIDATION

Using Matlab, we implement all the formulas that help us to calculate the value of the forces along x and y directions and the deviation angle δ. At the same interface, the program displays some others values that help us to understand the physical phenomena behind the fluidic injection in the divergent. Fig 9 is an example of the output of this program. This program gives us the possibility to choose different separation criteria in the computation of x_s.

We will use the results published by Zmijanovic and M.Sellam [5] to validate our analytical model . The validation is conducted with a conical type of the C-D axisymmetric nozzles of designed nozzle pressure ratios NPR = 37,5, throat radius of 9,72mm and expansion ratio $\frac{A_c}{A_e} = 0.236$ and the divergent conical half-angle of 5.42deg. The circular $b = 6mm$ diameter injection port is normal to the nozzle axis and at $\frac{x_m}{x_t} = 0.9$
Therefore, the value of the NPR is kept in the design adapted regime of NPR=37.5 while the SPR is varied. These results are presented in Table I.

World Academy of Science, Engineering and Technology
International Journal of Aerospace and Mechanical Engineering
Vol:9, No:7, 2015

TABLE I: Analytical, Numerical And Experimental Values Of δ.

$\frac{x_m}{x_t} = 0.9$				
SPR	f_m	δ-Model	δ-Num	δ-Exp
0.667	0.055	5.49°	5.67°	5.6°
0.833	0.068	6.79°	6.64°	6.7°
1	0.081	8.04°	8.05°	8.2°
1.167	0.098	9.23°	9.15°	9.2°
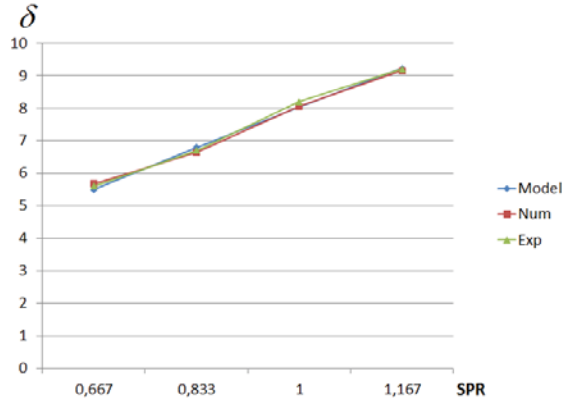
Fig. 10. δ versus SPR.

TABLE II: Absolute Error Between The Analytical And Numerical Values Of δ.

δ-Model	δ-Num	Error = $\mid \delta$-Model-δ-Num$\mid$
5.49°	5.67°	0.18°
6.79°	6.64°	0.15°
8.04°	8.05°	0.01°
9.23°	9.15°	0.08°

The analytical, numerical, and experimental results are plotted together in Fig. 9

At the Fig. 10 which depicts vectoring versus SPR (mass-flow ratio), optimal angle is found in the range of $SPR = 1$ delivering the $\delta = 8.049$. To understand deeply the validation of the 3D-analytical model, we calculated the deviation angle δ for different separation criteria. The Table III resume all the values of the deviation angle δ computed for five different separations criteria and compared with the numerical and experimental values.

TABLE III: Analytical For Different Separation Criteria, Numerical And Experimental Values Of δ.

SPR	0.667	0.833	1	1.167
δ-Model - Schilling	5.29	6.53	7.77	8.99
δ-Model - Zukoski	5.49°	6.79°	8.04°	9.23°
δ-Model - Summerfield	5.32	6.57	7.78	8.97
δ-Model - Stark	5.19	6.43	7.63	8.84
δ-Model - Schmuker	5.34	6.61	7.84	9.04
δ-Num	5.67°	6.64°	8.05°	9.15°
δ-Exp	5.6°	6.7°	8.2°	9.2°

We remark that the choice of the separation criteria has some influence in the computation of the deviation angle and the best separation criteria to choose is Zukoski criteria. Big majority of the results was in excellent agreement with the numerical and the experimental data. Numerical studies
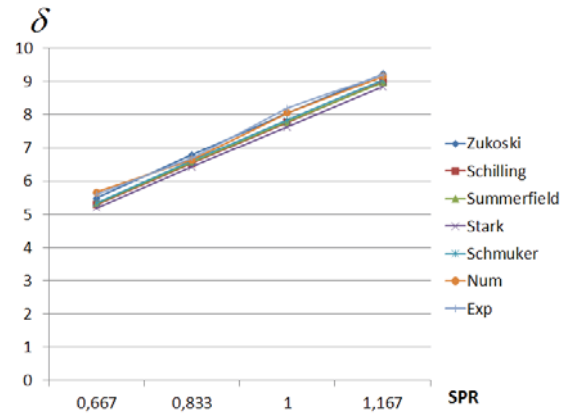

Fig. 11. δ versus SPR for different separation criteria.

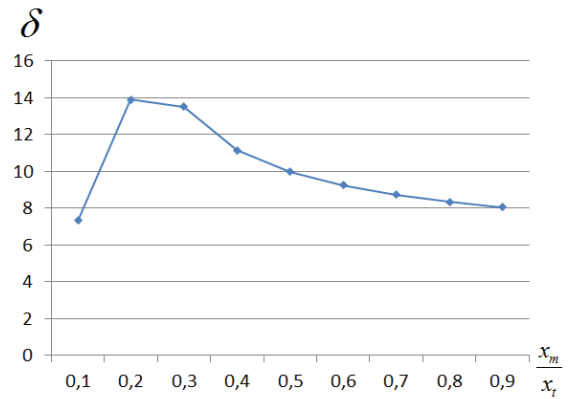Fig. 12. δ versus the location of the secondary injection.

have been carried out by Rajendran *et al.* [6] for the design optimization of a thrust vector control system for aerospace applications and they study the effect of the location of the secondary injection nozzle. Parametric analytical studies have been carried out with various secondary jet pressures at different divergent locations as shown in Table IV.

TABLE IV: Value Of δ While Varying The Location Of The Secondary Injection.

NPR = 37.5 SPR=1	
$\frac{x_m}{x_t}$	δ-Model - Zukoski
0.1	7.33°
0.2	13.9°
0.3	13.5°
0.4	11.15°
0.5	9.96°
0.6	9.25°
0.7	8.73°
0.8	8.34°
0.9	8.049°

The parametric studies show that the sonic secondary jet nozzle fixed at a location around 20% of the divergent nozzle length away from the nozzle exit will facilitate better thrust vectoring.

V. Conclusion

The analytical model shows that the deviation angle depends on many parameters such as the mass-flow rate, position and shape of the injector, angle of the secondary injection, and pressure ratios NPR and SPR. The efficiency and validity of the developed model, taking the numerical and experimental data from the literature, has been proved under various separation criteria with good accuracy. Further, fixing the sonic secondary jet nozzle at a distance around 20% of the total divergent nozzle length away from the exit boundary could facilitate better thrust vectoring for supersonic aerospace vehicles. As perspective to our investigation, the obtained analytical model including boundary conditions is useful in tackling to the guidance control problem.

References

[1] Balu, R., "Analysis of Performance of a Hot Gas Injection Thrust Vector Control System", Journal of Propulsion and Power, Vol. 4, pp.580-585, 1991.
[2] Spaid, F.W., and Zukoski, E. E., "Study of the interaction of gaseous jets from transverse slots with supersonic external flows", AIAA J. 6(2), pp.205.12., 1968.
[3] Spaid, F.W., and Zukoski, E. E., and Rosen, R., "A study of Secondary Injection of gases into a Supersonic Flow", Technical Report 32-834, NASA, 1966.
[4] Billig, F.S., J. "Shock-wave shapes around spherical- and cylindrical-nosed bodies", Journal of Spacecraft and Rockets, Vol.4 No.6, 1967.
[5] Zmijanovic,V., Lago, V., Leger, L., Depussay, E., Palerm, S., Oswald, J., Sellam, M., and Chpoun, A., "Thrust vectoring effects of a transverse gas injection into a supersonic cross-flow of an axisymmetric C-D nozzle", 4th European Conference for Aerospace Sciences (EUCASS), St. Petersburg, Russian, July 4-8, 2011.
[6] Rajendran, S. S., Aravind Kumar, T.R, Nareshkumar K.S, Ragothaman. S, Raveendran, R., and Sanal Kumar.V.R, "Studies on Thrust Vector Control using Secondary Injection Sonic and Supersonic Jets", 2nd Int. Conference on Mechanical, Electronics and Mechatronics Engineering (ICMEME'2013) June 17-18, London (UK), 2013.
[7] Mangin B., "Vectorisation fluidique de la pousse d'une tuyre plane supersonique". PhD thesis, Universit d'Orleans, Decembre 2006.
[8] Hefner, J. N., and Sterrett, J. R., "Secondary jet interaction with emphasis on outflow and jet location", AIAA J.Spacecr. Rockets, 09(11), pp.845-847, 1972.
[9] Avduevskii, V. S., Medvedev, K. I., and Polyanskii, M. N., "Interaction of a supersonic flow with a transverse jet injected through a circular aperture in a plate", Fluid Dynamics J., 5(5):888-891, 1970.
[10] Vlagov, V.V., Masayakin, N. E. , and Polyanskii, M. N., "Penetration depth of a jet injected into an oncoming supersonic flow", Fluid Dynamics J., 15(4), pp.599-602, 1980.
[11] Maarouf N., Sellam M., Grignon M., Chpoun A., "Thrust vectoring through fluid injection in an axisymmetrical supersonic nozzle", ISSW26 2, pp.1141-1147, 2007.
[12] Sellam M., Chpoun A., Zmijanovic V., Lago V., "Fluidic thrust vectoring of an axisymmetrical nozzle: an analytical model", Int. J. of Aerodynamics, Vol.2, No.2/3/4, pp.193 - 209, 2012.
[13] Schetz F.W., Billig E.E., "Penetration of gaseous jets injected into a supersonic stream", AIAA Journal Vol.3, No.11, pp.1658-1665, 1966.
[14] Neilson J.H., Gilchrist A., Lee C.K., "Side thrust control by secondary gas injection into rocket nozzles", Journal Mechanical Engineering Science Vol. 10, No.3, pp.239-251, 1968.
[15] Guhse R.D. "On secondary gas injections into supersonic nozzles", AIAA Journal Vol.3 No.1, pp.147-149, 1966.
[16] Dussauge J.-P., "Compressible turbulence in interaction of supersonic flows", Springer Turbulence and Interactions NNFM 105, pp.35-54, 2009.